A burden-free gene overexpression system

Carlos Barajas[1], Jesse Gibson[2], Luis Sandoval[3], and Domitilla Del Vecchio[1,*]

[1] Department of Mechanical Engineering, Massachusetts Institute of Technology, Cambridge, Massachusetts

[2] Department of Bioengineering, Stanford University, Palo Alto, California

[3] Department of Chemical Engineering, Massachusetts Institute of Technology, Cambridge, Massachusetts

[*] Correspondance: ddv@mit.edu

Abstract

Overexpression of synthetic genes depletes cellular resources, particularly ribosomes, which leads to lower expression of other synthetic genes and decreased growth rate. These burden effects can be detrimental to genetic circuit performance and hinders the process of modularly composing genetic circuits to create complex biomolecular systems with novel functions. No solution exists that allows the expression of any gene to a desired level without hindering the expression level of all other genes and growth rate. Here, we engineer an actuator that upregulates ribosome production. The key component of the actuator is a genetic cassette that expresses the hydrolysis domain of the SpoT enzyme (SpoTH) in a cell strain with elevated basal levels of ppGpp. We demonstrate that our actuator is capable of increasing protein production rates (proxy for free ribosomes) by over 150% and growth rate by over 80%. We use the actuator to engineer a feedforward controller, in which SpoTH is co-expressed with a target gene. Expressing the target gene without SpoTH purges the expression of a constitutive gene by more than 80% and cellular growth rate by 40%. By contrast, with SPOTH, the feedforward controller can be tuned to guarantee less than 10% change in the expression of a constitutive gene while keeping the expression of a the target gene at any desired level without any decrease in growth rate (however growth can increase by $\approx 40\%$). Alternatively, the feedforward controller can be tuned to guarantee less than 10% deviations in growth rate while also providing 30% higher expression of a constitutive gene relative to the case of expressing the target gene without SpoTH. Therefore, this solution allows desired target gene overexpression without burden, which is instrumental for predictable composition of genetic circuits.

Introduction

A challenge in synthetic biology is being able to modularly compose well-characterized genetic circuits to create complex systems [1, 2]. Contributing to this challenge are context-dependent effects, which include sharing of common cellular resources among genetic circuits. Specifically, it has been shown that ribosomes are a key limiting resource in protein production and can undesirably couple genetic circuits [3, 4, 5]. Overexpressing a gratuitous protein compromises the expression of a constitutively expressed gene and growth rate [6, 7, 8]. Decreased growth rates can compromise persistent overexpressoin of gene cassettes [9] or the coexistence of multiple strains in bacterial consortium applications [10, 11, 12].

An ideal solution to the ribosome sharing problem would allow for the expression of a gene cassette to any desired level without lowering the production rate of other genes and cell growth rate. Current solutions deviate from this ideal. For example, in [13], the mRNA production rate of a cassette is regulated using a burden sensitive promoter to maintain its production rate below the threshold that impacts the expression of constitutively expressed genes and cell growth. However, this design prevents the overexpression of the cassette to high levels. In [14], a synthetic 16S rRNA was used to allocate an orthogonal pool of ribosomes for synthetic mRNAs with a unique ribosome binding sequence (RBS) to guarantee orhtogonality. The expression of the synthetic 16S rRNA was regulated via a feedback mechanism to ensure the orthogonal ribosome pool is robust to the expression of synthetic mRNAs. Using the orthogonal pool fixes the RBS sequence, implying that designers lose a commonly used tuning parameter. Finally, in [15, 16] a feedback controller is appended to a gene of interest to ensure that its production rate is robust to ribosomes fluctuations. Nevertheless, this solution should be implemented for every gene to ensure that overexpression of a gene of interest does not affect expression of all other genes. Additionally, this solution does not address the issue of diminishing growth rate.

Ribosomes in *E. coli* are composed of three ribosome RNAs (rRNA) and more than 50 proteins (r-proteins) [17]. The transcription of rRNA is the rate-limiting step in ribosome production [18, 19] and is regulated based on the nutrient availability and current translational demand to yield the resource allocation that optimizes growth rate [20, 21, 22, 23, 24]. The concentration of r-proteins is autoregulated via translational inhibition [25, 17, 26] to stoichiometrically match rRNA levels since it is costly to manufacture r-proteins [27]. The production of rRNA is regulated by several protein factors [28, 29], iNTP [30, 31], and the two (p)ppGpp nucleotide analogs (abbreviated as ppGpp) [32, 33]. However, during balanced exponential growth, ppGpp is the primary regulator [18, 34, 35] and there is an inverse relationship between basal ppGpp levels and rRNA transcription (and growth rate) [36, 37, 38, 39]. The RelA/SpoT Homologue (RSH) proteins are responsible for the synthesis and hydrolysis of ppGpp [40, 41, 42] as shown in Fig. 1-a. The SpoT enzyme is bifunctional with both synthesis and hydrolysis capabilities (the latter dominating in exponential growth [43]), while the RelA enzyme is monofunctional with solely synthesis activity. Furthermore, SpoT is responsible for maintaining basal ppGpp levels in steady state growth [44].

In this work we leverage the ppGpp pathway to create a ribosome/growth rate actuator. By exogenously expressing the hydrolysis domain of SpoT [45], which we coin as SpoTH, we catalyze hydrolysis of ppGpp and thus upregulate ribosome production and growth rate (Fig. 1-a). We demonstrate that our actuator is capable of increasing the production rate of a constitutively expressed gene (a proxy for free ribosomes [8]) by over 150% and growth rate by over 80%. We apply our actuator to cancel the burden from overexpressing a target gene by creating a feedforward controller . The controller can be tuned to guarantee less than 10% deviations in constitutive gene expression as the target gene is expressed without any decrease in growth rate. Alternatively, the controller can be tuned to guarantee less than 10% deviations in growth rate while also providing 30% higher constitutive gene expression relative to the uncontrolled system. Our solution does not compromise the expression of the target gene, which can be expressed at any desired level without substantially compromising expression of other genes or growth rate.

Results

Actuating ribosomes and growth rate via spoTH

To actuate free ribosomes and growth rate we express spoTH (Fig. 1-a) from a genetic circuit. The spoTH gene (sequence shown in SI Table 1) encodes for only the first 203 spoT amino acids to guarantee only ppGppase activity [45]. The desired actuation profile of free ribosomes and growth rate as spoTH is expressed, is shown in Fig. 1-b, where an initial increase in spoTH concentration leads to an increase in both free ribosomes and

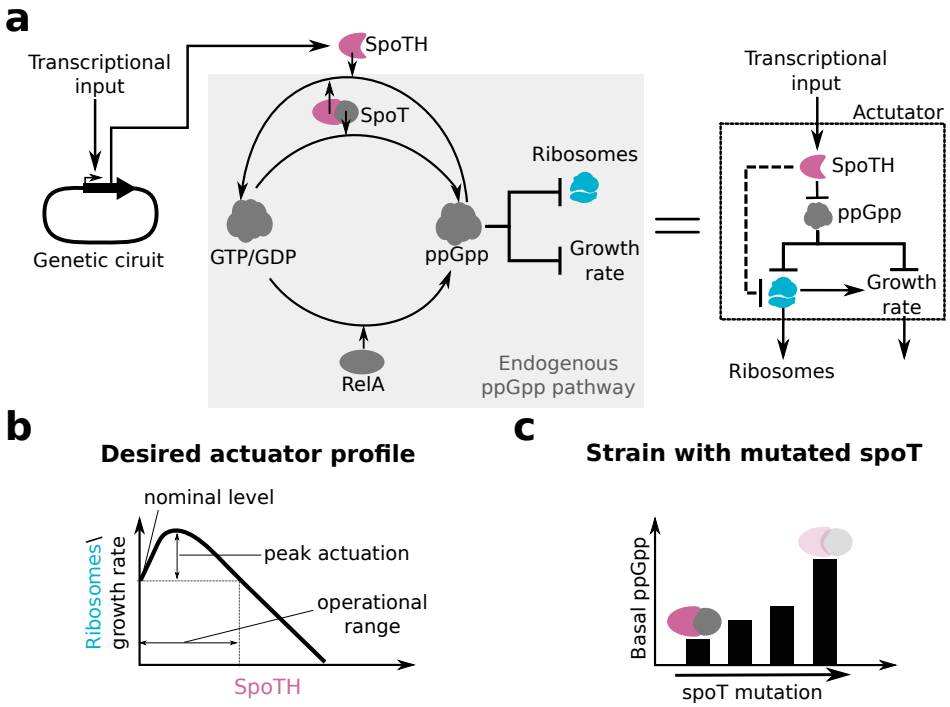

Figure 1: **Actuating free ribosome and growth rate via SpoTH** (**a**) The basal level of the nucleotide ppGpp sets ribosome production rate and growth rate in *E. coli* during exponential growth through a repression mechanism. The synthesis of ppGpp is catalyzed from GTP/GDP by RelA and the synthesis domain of SpoT (denoted in gray), while the hydrolysis of ppGpp is catalyzed by the hydrolysis domain of spoT (denoted in pink). By expressing the hydrolysis domain of spoT (spoTH) from a genetic circuit, we hydrolyze ppGpp and hence upregulate ribosome production and growth rate. Thus, spoTH expression serves as an actuator of ribosomes and cell growth. (**b**) The desired actuator profile is one where ribosome concentration and growth rate initially increase as spoTH is expressed. We define the nominal ribosome/growth rate level as the level when there is no SpoTH present. Since the ribosomal cost to translate spoTH continues to increase as more mRNA is produced but upregulation of ribosome production saturates when most of the ppGpp in the cell has been hydrolyzed, we expect that the actuator profile will peak (we define the ribosomal/growth rate level at this peak as the peak actuation) and decrease as spoTH expression increases. We refer to the SpoTH concentration where the actuator profile drops back to the nominal level as the operational range. In application, SpoTH expression should be kept within the operational range to ensure positive actuation. (**c**) We probe several strains with endogenous spoT mutated (yielding varying levels of basal ppGpp) to guage if expressing spoTH results in the desired actuation profile.

growth rate. In the first part of this section we probe several strains (as shown in Fig. 1-c) to choose one that yields the desired actuation profile. Then, we show that for the strain with the desired actuation properties, we can tune the actuation profile using different carbon sources and demonstrate a trade-off between peak actuation and nominal ribosome/growth rate levels.

Choosing strain with desired actuator profile

The genetic circuit used to express spoTH is shown in Fig. 2-a. We can increase the concentration of SpoTH by increasing the concentration of the aTc inducer. We use the production rate of GFP as a proxy for free ribosomes [46]. We probe four different strains to gauge if they render the desired actuation profile when used as the chassis to express spoTH. We test the wild type MG1655 strain along with a set of strains with spoT mutated to render varying levels of basal ppGpp/nominal growth, these are: CF944 (*spoT202* allele), CF945 (*spoT203* allele), and CF946 (*spoT204* allele) [36, 47, 48, 34].

The results from expressing SpoTH (using the construct in Fig. 2-a) in these strains and monitoring the production rate of a constitutively expressed green fluorescent protein (GFP) and growth rate, are shown in Fig. 2-C and Fig. 2-D, respectively. For MG1655 (CF944) we can actuate GFP by 22% (45%), but not

growth rate. For CF945, we can actuate GFP by 90% and growth rate by 80%. For CF946, GFP initially decreases, but then increases by 65% (relative to 0 aTc) and growth rate increases by 60%. Therefore, CF945 is the only strain that provides the desired actuation profile (Fig. 2-b) for both free ribosomes (GFP production rate) and growth rate and thus it is the strain we work with for the rest of this study. Notice that the GFP production rate and growth rate actuator profiles don't fully correlate. For example, for CF945, GFP production rate peaks at aTc $\approx$ 215 nM and then begins to decrease, while growth rate continues to increase. This lack of correlation between GFP production rate and growth rate is expected since growth rate depends on an ensemble of endogenous proteins [21, 49, 22, 50] and not solely on free ribosomes.

From Fig. 5 in Box 1, our simple mathematical model predicts that depending on the parameter regime, the actuation profile can: (I) have the qualitative behavior as our desired profile, (II) continuously decrease as spoTH is increased (similar to the growth rates of MG1655 and CF944), (III) initially decrease and then increase (like the GFP production rate of CF946). From Remark 1 in Box 1, having too little basal ppGpp (like MG1655/CF944) or too much (like CF946), can place the parameters outside the regime that renders the desired actuation profile. Thus it supports our findings that the intermediate strain CF945, with just the right amount of basal ppGpp, renders the desired actuator profile.

Tuning actuation profile via carbon source and trade-off between nominal growth and maximum actuation potential

The CF945 strain provides the desired actuation profile (both for GFP production rate and growth rate), however, we would like a simple method to tune the profile while using this chassis. It has been shown that the culture media composition, specifically carbon source, can determine the ppGpp basal level/nominal growth rate [37, 51, 22, 35, 52]. Therefore, we propose tunning the properties of the actuation profile (Fig. 1-b) in CF945 by varying the carbon source.

We express spoTH (genetic circuit Fig. 2-a) using four commonly used carbon sources: lactose, glycerol, fructose, and glucose. The normalized GFP production rate (with respect to GFP at 0 aTc) is shown in Fig. 2-d. The GFP production rate at 0 aTc (nominal GFP production rate) vs the normalized peak GFP actuation for each carbon source along is shown in Fig. 2-e. We observe that all carbon sources yield the desired actuation profile and that there is an inverse relationship between the normalized peak actuation and the nominal production rate. The nominal GFP production rate hierarchy is fructose>glucose >glycerol >lactose, while the peak actuation hierarchy is fructose$\approx$glucose<glycerol <lactose. The nominal GFP production rate for fructose is 2.6 times higher than that of lactose, but in lactose, the GFP production rate can be actuated by 150% compare to just 50% for fructose.

The normalized growth rate (with respect to 0 aTc) is shown in Fig. 2-f. The growth rate at 0 aTc (nominal growth rate) vs the normalized peak growth rate actuation for each carbon source is shown in Fig. 2-g. We observe that for all carbon sources, the growth rate increases with spotH expression (aTc). The nominal growth rate hierarchy is glucose> fructose> >glycerol >lactose, while the peak actuation hierarchy is glycerol >lactose>fructose> glucose. For glycerol the nominal growth rate is $\approx$ 0.2 1/hr with a peak actuation of $\approx$ 85%, while for glucose the nominal growth rate is $\approx$ 0.35 1/hr with a peak actuation of $\approx$ 45%.

The results from Fig. 2-e and Fig. 2-g suggest that there is a tradeoff between nominal levels and relative actuation. Intuitively, this tradeoff occurs because if lower nominal GFP production rate/growth rate levels are due to high basal ppGpp levels, then this implies that there is more ppGpp available to hydrolyze and thus actuate. Our physical intuition is made mathematically precise in Box 1. In Fig. 6 in Box 1, we demonstrate that our model predicts the tradeoff between the nominal level of free ribosomes vs the relative peak actuation of free ribosomes. The model predicts that lower nominal ribosome levels lead to higher relative peak actuation up until a certain critical value (as observed for growth rate in Fig. 2-g). Below the critical value, relative peak actuation decreases with nominal free ribosomes level.

Actuator application: Cancel burden arising from heterologous protein overexpression

Overexpressing a heterologous protein decreases protein production rates and cell growth rate [6, 4, 53] due to the depletion of ribosomes available to translate mRNA. This motivates us to apply our actuator to cancel these two burden effects from gene overexpression. The first part of this section will assess the capabilities of our actuator to rescue protein production rates and growth rate as a red fluorescent protein (RFP) is

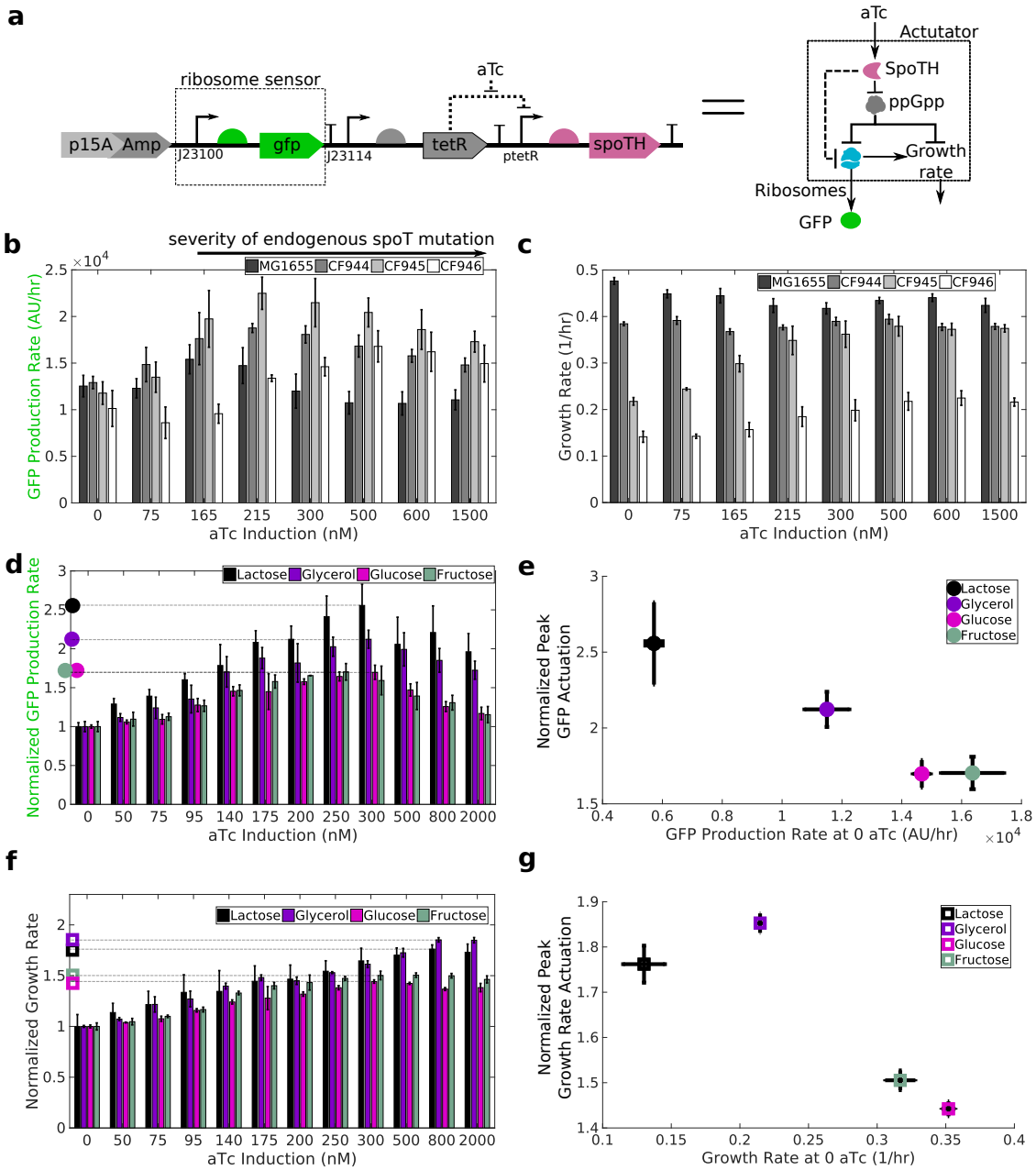

Figure 2: **Expressing spoTH in several strains to acquire the desired actuation profile and tunning the profile using four different carbon sources.** **(a)** The genetic construct used to express spoTH using inducible ptetR promoter and measuring growth rate and GFP production rate (proxy for free ribosomes). **(b)/(c)** The GFP production rate/growth rate while expressing SpoTH (increase aTc) in the MG1655, CF944, CF945, and CF946 strains in M9 media supplemental with glycerol. **(d)** The normalized GFP production rate as spoTH is expressed in CF945 growing in M9 media supplemented with lactose, glycerol, fructose, or glucose. The normalized peak GFP actuation is denoted by closed circles. **(e)** The normalized peak GFP actuation versus the GFP production rate at 0 aTc (nominal production rate) for each carbon source. **(f)** The normalized growth rate as spoTH is expressed in CF945 growing in M9 media supplemented with lactose, glycerol, fructose, or glucose. The normalized peak growth rate actuation is denoted by open squares. **(g)** The normalized peak growth rate actuation versus the growth rate at 0 aTc (nominal growth rate) for each carbon source. For all data, error bars represent standard deviation from at least four replicates (two biological replicates each with two technical replicates). The unnormalized data is shown SI Fig. 9.

overexpressed. Next, to automate the process of canceling the burden of expressing RFP, we place both the RFP and SpoTH under the same inducible promoter (feedforward configuration) and tune the spoTH RBS to flatten the response curve between RFP produciton rate and free ribosomes/growth rate.

The actuator is capable of rescuing burden caused by overexpressing RFP

To assess the capability of the spoTH actuator to rescue the protein production rate of a constitutive expressed gene (proxy for free ribosomes) and growth rate when these are reduced through heterologous protein expression, we expresses SpoTH and the burden protein RFP under two separate inducible promoters as shown in Fig. 3-a. From Fig. 3-b, the addition of AHL will initiate the production of rfp mRNA and hence sequester free ribosomes, which causes a decrease in the rates of GFP production and growth. The addition of aTc will produce SpoTH and thus upregualte GFP production rate and growth rate in a manner as observed in Fig. 2.

From Fig. 3-c, we observe that for 0 aTc (no spoTH expression) as RFP increases (increasing AHL) GFP production rate drops up by $\approx 80\%$. However, increasing aTc (spotH expression), rescues GFP production rate back to the nominal value (GFP production rate at AHL = 0 and aTc = 0). For each aTc value, we show the RFP production rate value for which GFP production rate is rescued back to the nominal value. For aTc = 250 nM, the actuator rescues GFP production rate from a decrease of over 60%. From Fig. 3-d, we observe that for 0 aTc (no spoTH expression) as RFP increases (increasing AHL) growth rate drops up to $\approx 35\%$. However, increasing aTc (spotH expression), rescues growth rate back to the nominal value (GFP production rate at AHL = 0 and aTc = 0). We show explicitly for each aTc value, the RFP production rate value for which GFP production rate is rescued back to the nominal value. For aTc = 105 nM, the actuator rescues growth rate from a decrease of $\approx 35\%$. In Fig. 3-e we plot the aTc induction vs RFP production rate path that perfectly rescues GFP and growth rate. The paths are made continuous by linearly interpolating the data in Fig. 3-c and Fig. 3-d. We observe that the path to rescue GFP and growth rate are not identical. This implies that it may not be possible to perfectly rescue GFP production rate and growth rate simultaneously. Due to the lack of correlation between GFP production rate and growth rate as spoTH is expressed (Fig. 2), this is expected.

The results from Fig. 3-c are in qualitative agreement with our mathematical model (Fig. 7 in Box 2). Our model predicts that we can cancel the reduction in free ribosomes as a heterologous protein is expressed.

Feedfoward controller to cancel the burden from heterologous protein overepxression

The results from Fig. 3 suggest that for every level of RFP, there exists an amount of spoTH mRNA to perfectly rescue GFP production rate back to the nominal level and a different amount of spoTH mRNA to perfectly rescue growth rate back to the nominal level (Fig. 3-e). On the field, it may be difficulty to separately tune the expression of RFP (or any other protein of interest) and SpoTH to cancel burden effects. Here, we automate the process of simultaneously expressing rfp and spoTH mRNA as shown in Fig. 4-a. Both rfp and spoTH are activated by the same transcriptional signal and the branch that goes through RFP hinders ribosomes/growth rate while the branch that goes through SpoTH upregulates ribosomes/growth rate (if the actuator is within the operational range). This architecture is known as a feedfoward controller. We refer to the open loop (OL) when the transcription (TX) signal only activates RFP and the closed loop (CL) when it actives both RFP and SpoTH. In Fig. 4-b we show the expected OL response as RFP is expressed (this should be similar to the 0 aTc case in Fig. 3), the ideal response where GFP production rate and growth rate remain constant as RFP is expressed, and the expected CL responses. The genetic circuit implementations of the OL and CL are shown in Fig. 4-c and Fig. 4-d, respectively. We tune the SpoTH ribosome binding site (RBS) of the CL to try an approximate the ideal response. We also consider a control genetic circuit as shown in Fig. 4-e, where we replace SpoTH with CJB (a nonfunctional heterologous protein). This control circuit allows us to verify that the CL performs better than the OL due to the actuation properties of SpoTH and not because of the configuration change that the RFP mRNA undergoes when it is coexpressed with a second protein.

As shown in SI fig. 16, we design four SpoTH RBS's to tune the CL response. In Fig. 4-f we show the normalized (with respect to 0 AHL) GFP production rate as RFP is expressed when using lactose as the carbon source, for the control circuit, the OL, and the RBS library of the CL. For the CL with RBS 3, we can approximate the ideal curve within 10% error for all the RFP values achieve by the OL, while the OL GFP drops by over 80%. In Fig. 4-g we show the normalized (with respect to 0 AHL) growth rate as RFP is expressed when using lactose as the carbon source. For the CL with RBS 2, we can approximate the ideal

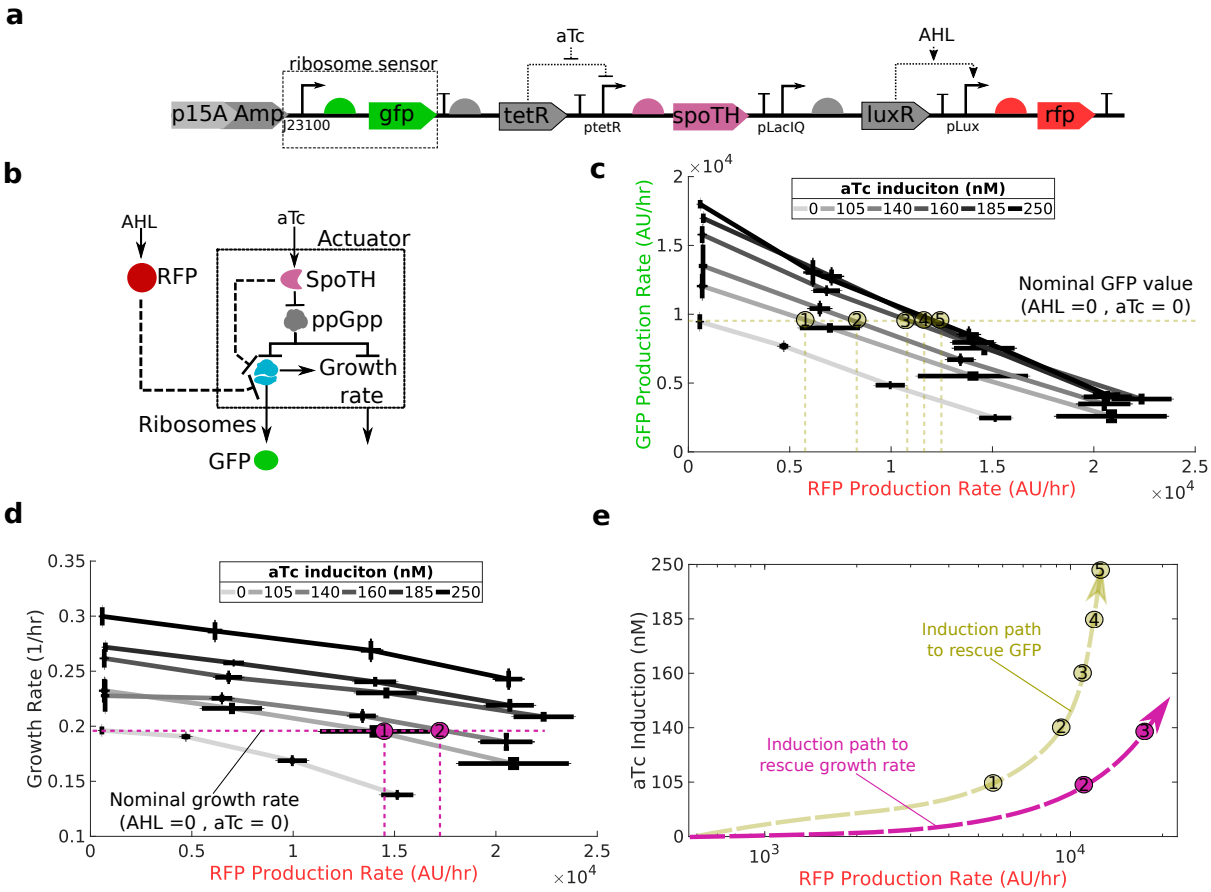

Figure 3: **SpoTH actuator rescues reduced protein production rate and growth rate due to overexpressing a heterologous protein.** **(a)** The genetic construct used to express SpoTH and RFP under two sepereate inducible promoters. This circuit is identical to the one in Fig. 2-a, but with the addition of RFP under the inducible plux-luxR promoter. **(b)** AHL activates the production of RFP, which depletes free ribosome/growth rate levels. The addition of aTc will positively actuate free ribosomes and growth rate. Here we use the production rate of a constitutively expressed GFP as a proxy for free ribosomes. **(c)** The GFP production rate as RFP and SpoTH are induced. As RFP is expressed (increase AHL) GFP levels drop. But as SpoTH is expressed (increase aTc) it rescues GFP to the nominal level (aTc = 0 and AHL = 0). **(d)** The growth rate as RFP and SpoTH are induced. As RFP is expressed (increase AHL) growth rate drops. But as SpoT is expressed (increase aTc) it rescues growth rate to the nominal level (aTc = 0 and AHL = 0). **(e)** The RFP production rate vs aTc induction paths to rescue GFP production rate and growth rate (to the level when aTc = 0 and AHL = 0). The paths are made continuous by linearly interpolating the experimental data. Note that these two paths are not identical. For all data, error bars represent standard deviation from at least four replicates (two biological replicates each with two technical replicates). Glycerol was the carbon source used in all the experiments in this figure. The AHL concentrations used in this experiment were AHL = 0 nM, 3nM, 7nM, 15 nM.

curve within 10% error for all the RFP values achieve by the OL, while the OL GFP drops by over $\approx 40\%$. In SI Fig. 10 and Fig. 11, we show the unormalized AHL induction plots corresponding to Fig. 4-f and Fig. 4-g. As expected from Fig. 3-e, the RBS that best rescues GFP is not the same as the RBS that best rescues growth rate.

In Fig. 4-h we show the normalized (with respect to 0 AHL) GFP production rate as RFP is expressed when using glycerol as the carbon source. For the whole CL RBS library, the OL and CL are nearly identical (within error). In Fig. 4-i we show the normalized (with respect to 0 AHL) growth rate as RFP is expressed when using glycerol as the carbon source. For the CL with RBS 2, we can approximate the ideal curve within 10% error for all the RFP values achieve by the OL, while the OL GFP drops by over $\approx 40\%$. In SI Fig. 12 and Fig. 13, we show the unormalized AHL induction plots corresponding to Fig. 4-f and Fig. 4-g.

For all results in Fig. 4, the control performs worst than both the OL and CL as expected since we have the burden from both RFP and CJB without the SpoTH actuation. Here we only tried lactose and glycerol since from Fig. 3, they provide the most relative actuation.

The prediction from the mathematical model using the feedfoward controller are shown Box 2, Fig. 8. We demonstrate that if the parameter regime is such that the actuator has the desired response (like CF945 in Fig. 3), then the SpoTH RBS can be chosen such that in CL, ribosome levels stay constant (initially) as the heterologous protein is expressed. Furthermore, we show that even if the chosen CL RBS does not render constant ribosome concentration, it can still perform better than the OL.

Discussion

The alarmone ppGpp has been refereed to as the CEO of the cell, whose job is to optimally allocate resources for growth based on environmental conditions and current translational activity [50]. In this paper, we engineered an actuator that interfaces with ppGpp and upregulated protein production rates (proxy for free ribosomes) and cellular growth rate. The actuator's key mechanism is the expression of the hydrolysis domain of spoT (SpoTH) in a strain with high level of basal ppGpp (CF945). We demonstrated that by tuning the carbon source we could exploit the tradeoff between nominal growth and maximum actuation potential. For example, using glucose as the carbon source, the cells had a doubling time of 2 hours and the actuator could upregulate growth rate by $\approx 45\%$ (protein production rate by $\approx 60\%$). In contrast, with lactose as the carbon source, the cells had a doubling time of ≈ 5 hours and the actuator could upregulate growth rate by $\approx 75\%$ (protein production by $\approx 150\%$). In this work we choose to use carbon source to tune the basal level of ppGpp, but other methods such as tuning the amino acid concentration in the media [36] could be implemented.

We apply the actuator to cancel the burden from overexpressing a gene cassette by creating an incoherent feedforward loop (iFFL). Expressing RFP in an OL configuration purges the protein production rate of a constitutively expressed gene by more than 80% and cellular growth rate by 40%. We create an iFFL expressing spoTH on the same promoter as RFP. We tune the CL via the spoTH RBS to guarantee less than 10% deviations in protein production rates as RFP is increased to the same level as the OL. Hoverer, for this RBS wihtin the same RFP range, growth rate increases by 40%. Alternatively, the RBS can be chosen to guarantee less than 10% deviations in growth rate while also providing significantly higher constitutive protein production rates relative to the OL.

Our understanding of ppGpp (especially its role in exponential growth) is constantly evolving [50], so as we gain more insight on this pathway, it may provide opportunities to further optimize the actuator. Furthermore, other enzymes like mesh1 [54, 55] and SpoT E319Q [56] have been shown to catalyze the hydrolysis of ppGpp and can serve as alternative actuators. Furthermore, this work provides an example of exploiting endogenous pathways for synthetic biology applications. Finally, we implemented our actuator in a feedforward controller to cancel burden, but also applying it in a feedback configuration would be of interest.

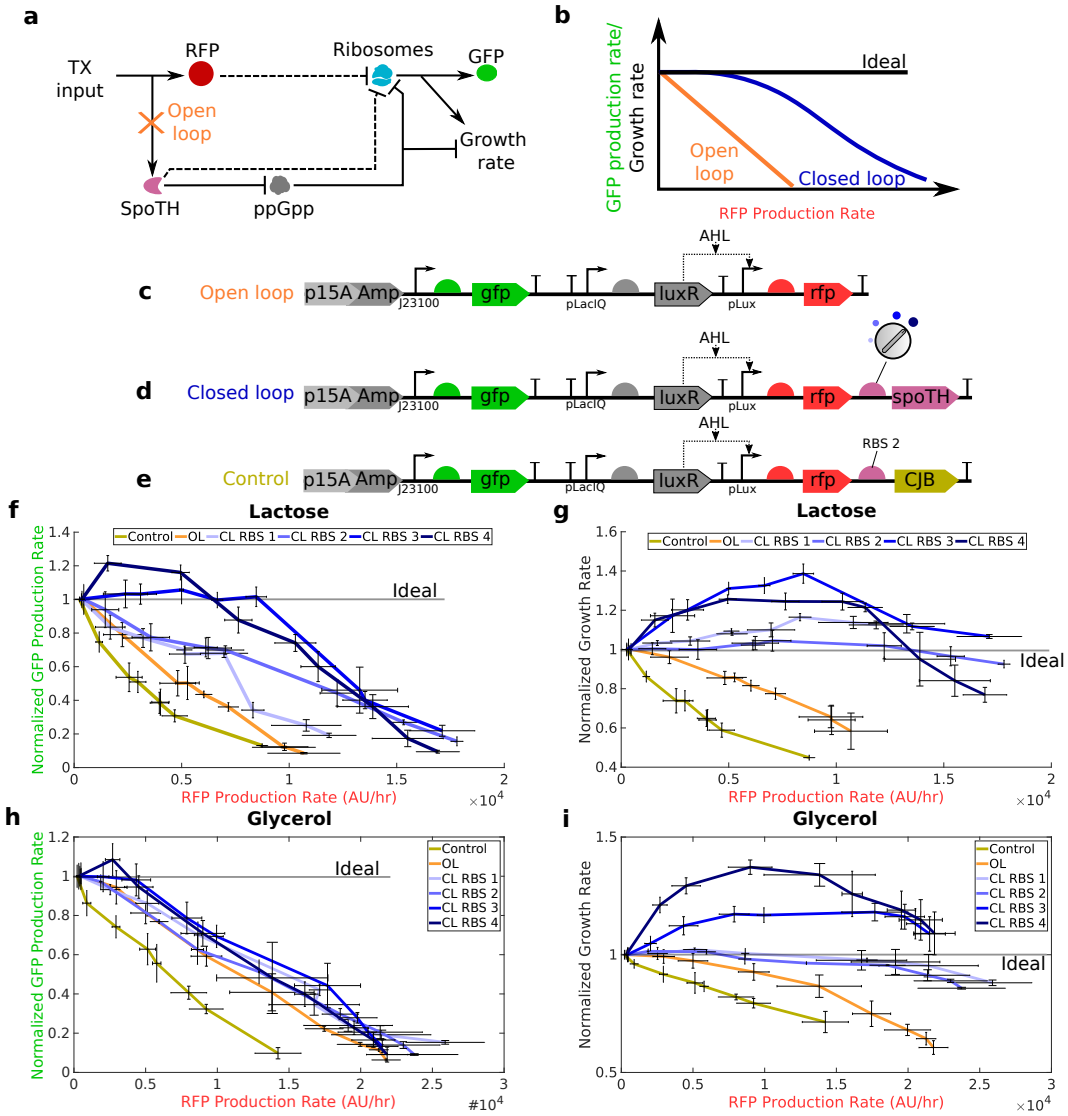

Figure 4: **Feedforward controller to automatically cancel the burden from expressing RFP.** **(a)** Open loop: A transcriptional (TX) input activate solely RFP produciotn, which which sequesters free ribosomes and hence hinders GFP production rate and growth rate. Closed loop: the TX input also activates SpoTH production and hence upregulates ribosome concentration. The closed loop is in a feedforward controller architecture. **(b)** The expected GFP production rate/growth rate as RFP is expressed for the ideal case where these quantities remain constant, the open loop, and the closed loop. **(c)** The open loop genetic construct used to express RFP under the inducible plux-luxR promoter while monitoring the constitutive expression of GFP (proxy of free ribosomes). **(d)** The closed loop genetic construct used to express RFP and SpoTH under the same inducible plux-luxR promoter. We vary the RBS of SpoTH to tune the closed loop response to approximate the ideal case. **(e)** The control genetic construct used to express RFP and CJB under the same inducible plux-luxR promoter. The CJB is a nonfunctional heterologous protein. **(f)** The GFP production rate vs RFP production rate for the control, open loop, and closed loop (for 4 RBS) when lactose is the media. **(g)** The growth rate vs RFP production rate for the control, open loop, and closed loop (for 4 RBS) when lactose is the media. **(h)** The GFP production rate vs RFP production rate for the control, open loop, and closed loop (for 4 RBS) when glycerol is the media. **(i)** The growth rate vs RFP production rate for the control, open loop, and closed loop (for 4 RBS) when glycerol is the media. For all data, error bars represent standard deviation from at least four replicates (two biological replicates each with two technical replicates). The unormalized data along with the AHL values used is shown in SI Fig. 10-SI Fig. 13.

Box 1 Actuator Model

Here we provide a simplified mathematical model that describes how expressing spoTH actuates free ribosome. The full model derivation and details can be found in SI Section: *SpoTH Actuator Model*. The key dimensionless equation describing how the total ribosome concentration equals the sum of the free ribosome concentration (R) and the concentration of ribosomes translating spoTH mRNA (c_s) is given by

$$\underbrace{\overbrace{R_0}^{\text{nominal } (c_s=0)} + \overbrace{(1-R_0)f(c_s/\epsilon, R_0)}^{\Delta\text{: spoTH actuation}}}_{\text{total ribosomes}} = R + c_s, \quad (1)$$

where $R_0 \in [0,1]$ is the nominal level of free ribosomes ($R_0 = R(c_s = 0)$) and Δ describes the actuation of ribosome production as spoTH is expressed, $f = \frac{(c_s/\epsilon)(c_s/\epsilon+2)}{(c_s/\epsilon)(c_s/\epsilon+2)+1/R_0}$, and ϵ is a dimensionless parameter that corresponds the rribosomal cost to express sufficient spoTH to degrade ppGpp (cost to actuate). A small ϵ implies that the amount of ribosomes needed to produce enough SpoTH to actuate (degrade a sufficient amount of ppGpp) is small compared to the increase in ribosomes due to ppGpp hydrolysis. In the derivation of (1), we accounted for the concentration of ribosomes translating endogenous mRNA, but this term is not explicit shown in (1) due to the nondimensionalization. The concentration of SpoTH is proportional to c_s and thus we use increasing SpoTH expression and increasing c_s interchangeably. An additional key quantity is

$$\delta(R_0, \epsilon) := \left.\frac{dR}{dc_s}\right|_{c_s=0} = 2\frac{R_0(1-R_0)}{\epsilon} - 1. \quad (2)$$

The qualitative behavior of (1) is shown in Fig. 5 and it has three prototypical responses. When $\delta > 0$, we get the desired actuator profile where R increases initially as c_s increases. As $\delta \to \infty$, the peak actuation and actuator operational range (as defined in Fig 1-b) both approach $(1-R_0)$. When $\delta < 0$, R decreases initially as c_s increases and then it can either continue to decrease or it can eventually increase past R_0, peak, and then decrease again.

Remark 1. From (2), for a fixed ϵ such that $\epsilon < 0.5$, there exists $0 < R_{0,*} < R_0^* < 1$ such that for all $R_0 \in (R_{0,*}, R_0^*)$ we have $\delta > 0$ and for all R_0 outside this set $\delta < 0$. In SI section: *SpoTH Actuator Model* (16), we show that R_0 monotonically decreases with basal ppGpp and this implies that for a fixed ϵ, there is also an open interval of basal ppGpp values that render the desired actuation profile. This implies that too high or too low basal ppGpp can be detrimental in achieving the desired actuator profile.

In Fig. 6, we show the normalized actuation (R/R_0) profile for $\epsilon = 0.13$ and $R_0 = 0.125, 0.25, 0.3, 0.34$. These parameters are chosen such that relative peak actuation and the ratio of nominal values math those of the GFP production rate data shown in Fig. 2-d and Fig. 2-e ($R_0 = 0.125$ for lactose, $R_0 = 0.25$ for glycerol, $R_0 = 0.34$ for glucose, $R_0 = 0.34$ for fructose). We observe that for lower R_0 we have more relative peak actuation. In the inset we show that show that the peak actuation increases as R_0 up until $R_0 \approx 0.1$. After this critical value peak actuation decreases as R_0 decreases.

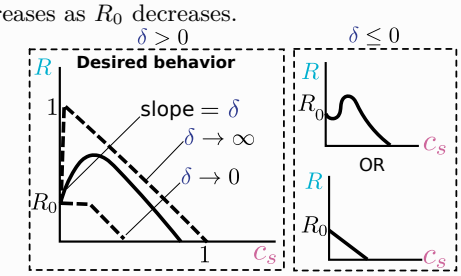

Figure 5: **Qualitative behavior of actuator** For $\delta > 0$ (given by (2)), the actuator profile predicted by (1) has the desired behavior where R increases as spoTH is expressed (increasing c_s), then it peaks and begins to drop. When $\delta < 0$, the amount of free ribosome initially decreases as SpoTH is expressed. It can then either continue to decrease or at some point increase, peak, and then decrease again.

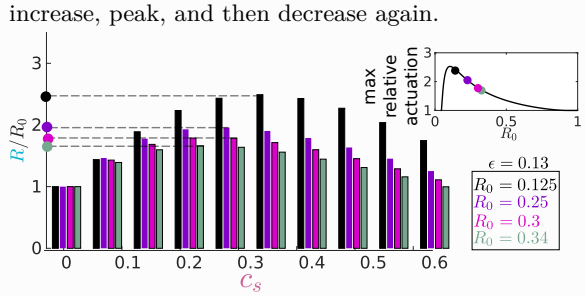

Figure 6: **Tradeoff between nominal level and relative peak actuation** The actuation profile predicted by (1) for several R_0. We observe that for lower R_0, there is higher peak actuation. In the inset we show that the peak actuation increases as R_0 up until $R_0 \approx 0.1$. After this critical value peak actuation decreases as R_0 decreases.

Box 2 Actuator to cancel burden from heterologous protein overexpression

We modify (1) in Box 1 to account for the expression of a heterologous protein y, which reads

$$R_0 + (1 - R_0) f(c_s/\epsilon, R_0) = R + c_s + c_y, \quad (3)$$

where c_y is the concentration of ribosomes translating y mRNA. The protein concentration of y is proportional to c_y. The quantities c_y and c_s are related to free ribosomes by

$$c_y = m_y R/K_y, \quad c_s = m_s R/K_s \quad (4)$$

where m_y is the y mRNA concentration, K_y is the dissociation constant of free ribosome with y mRNA, m_s is the spoTH mRNA concentration, and K_s is the dissociation constant of free ribosome with spoTH mRNA. As shown in Fig. 7, we set input 1 $= m_y/K_y$ and input 2 $= m_s/K_s$. As input 1 increases, free ribosome concentration decreases by 80%. For a fixed c_y, we can rescue R by increasing input 2. For example, by increasing input 1 such that $c_y = 0.14$, we have that R drops by 56%, but if input 2 $= 0.3$, we can fully rescue R back to R_0. For this simulation $R_0 = 0.25$ and $\epsilon = 0.13$, by looking at Fig. 6 we observe that for this parameters the maximum relative actuation is $\approx 100\%$. Furthermore, in the simulation the maximum value for input 1 was 3.2 regardless of the value of input 2, but as input 2 increases the maximum values of c_y achieved increase. This implies that for a fixed amount of y mRNA, increasing input 2 increases the amount of protein y produced.

To automate the process of rescuing free ribosomes as y is expressed, one can transcriptionally couple its expression with that of SpoTH by having them under the same promoter, which implies that $m_y = m_s$ and thus $c_s = \gamma c_y$ where

$$\gamma = K_y/K_s. \quad (5)$$

We refer to the configuration where y and spoTH are transcriptionally coupled as the closed loop and obeys (3) with $c_s = \gamma c_y$. We denote expressing y in the absence of spotH as the open loop and it obeys (3) with $c_s = 0$. One can tune γ in the closed loop to try and approximate the ideal scenario where $R = R_0$ for all c_y, as shown in Fig. 8. The initial slope ($\frac{dR}{dc_y}|_{c_y=0}$) of the closed loop is given by $\gamma\delta - 1$ (see qualitative behavior in SI Fig. 15). Thus, if we choose $\gamma = 1/\delta(R_0, \epsilon)$, then ribosome levels initially remain constant as y is expressed. Note that since γ represents that ratio of the RBS strengths of spoTH and y, then it must be a positive quantity. Therefore, to choose $\gamma = 1/\delta(R_0, \epsilon)$, we must have $\delta > 0$, which from Fig 5, implies that we are in the parameter regime such that the actuator has the desired profile.

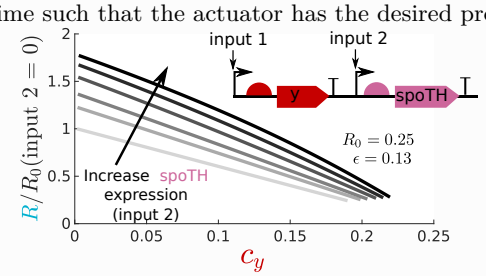

Figure 7: **SpoTH can rescue the drop in free ribosomes from heterologous protein overexpression** Simulation of (3) when protein y and SpoTH are under the control of diffrent inputs. As input 1 increases R drops, but for a fixed c_y, the ribosome level ran be rescued to back to R_0 by expressing SpoTH (input 2). Here input 1 ranges from 0 to 3.2 and input 2$= 0, 0.10, 0.15, 0.21, 0.26, 0.3$.

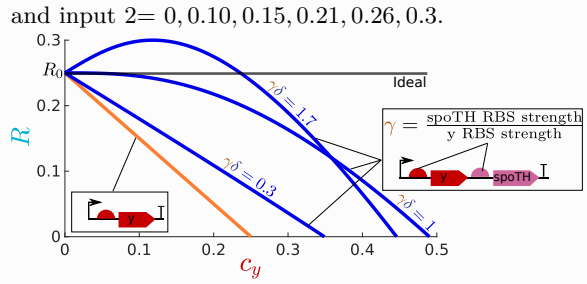

Figure 8: **Transcriptionally couple** y **and spoTH to automatically cancel burden from protein overexpression** Simulation of (3) with $c_s = \gamma c_y$. This corresponds to placing y and SpoTH under same promoter (closed loop). The spoTH RBS (γ) can be tuned to approximate the ideal scenario where $R = R_0$ for all c_y. We also show the open loop (y without spoT) in orange given by (3) with $c_s = 0$. For this simulation $\epsilon = 0.13$

Acknowledgements

We thank Hsin-Ho Huang for helping guide the plasmid construction. We thank Dr. Chasel, Dr. Potrykus, and Dr. Fernández-Coll for providing the CF944, CF945, and CF946 strains and their helpful discussion on ppGpp.

Materials and Methods

Bacterial strain and growth medium

The bacterial strain used for genetic circuit construction was *E. coli* NEB10B (NEB, C3019I) and LB broth Lennox was the growth medium used during construction. Characterization was performed using the CF944, CF495 , and

CF946 strains [36] and the MG1655 strain (CGSC, 6300). Characterization experiments were done using M9 minimal medium supplemented with 0.2% casamino acids,1 mM thiamine hydrochloride, ampicillin (100 μg/mL), and either 0.4% glucose, 0.4% fructose, 0.4% glycerol, or 2 g/L lactose (the specific carbon source used for each experiment is specified in the figure caption).

Microplate photometer

Cultures were prepared by streaking cells from a 15 % glycerol stock stored at $-80°$C onto a LB (Lennox) agar plate containing 100 μg/mL ampicillin and incubated at 37°C for 16 hours. Isolated colonies were picked and grown in 2 ml of growth medium in culture tubes (VWR, 60818-667) for 12-24 hours at 30°C and 220 rpm in an orbital shaker. Cultures were then diluted to an OD at 600 nm ($\mathrm{OD}_{600\mathrm{nm}}$) of 0.0075 in 4 mL and grown for an additional 6 hours in culture tubes (VWR, 60818-667 to ensure exponential growth before induction. Cultures were then induced and plated onto 96 well-plate (Falcon, 351172). The 96-well plate was incubated at 30°C in a Synergy MX (Biotek, Winooski, VT) microplate reader in static condition and was shaken at a fast speed for 3 s right before OD and fluorescence measurements. Sampling interval was 5 minutes. Excitation and emission wavelengths to monitor GFP fluorescence are 485 and 530 nm, respectively and those to monitor RFP fluorescence are 584 and 619 nm, respectively.

Genetic circuit construction.

The genetic circuit construction was based on Gibson assembly CITE. DNA fragments to be assembled were amplified by PCR using Phusion High-Fidelity PCR Master Mix with GC Buffer (NEB, M0532S), purified with gel electrophoresis and Zymo clean Gel DNA Recovery Kit (Zymo Research,D4002), quantified with the nanophotometer (Implen, P330), and assembled withGibson assembly protocol using NEBuilder HiFi DNA Assembly Master Mix(NEB, E2621S). Assembled DNA was transformed into competent cells prepared by the CCMB80 buffer (TekNova, C3132). Plasmid DNA was prepared by the plasmid miniprep-classic kit (Zymo Research, D4015). DNA sequencing used Quintarabio DNA basic sequencing service. Primers and gBlocks were obtained from Integrated DNA Technologies. The list of constructs and essential DNA sequences can be found in SI Table 1.

Calculating growth rate and protein production rates

The background OD (0.08 $\mathrm{OD}_{600\mathrm{nm}}$) and GFP (100 AU) were subtracted from the data prior to any calculations. To ensure the data analyzed was coming from cells in exponential growth, only OD values (adjusted for background) of $\mathrm{OD}_{600\mathrm{nm}} = 0.06$ and $\mathrm{OD}_{600\mathrm{nm}} = 0.14$ were considered except for experiments done in lactose were the range was $\mathrm{OD}_{600\mathrm{nm}} = 0.06$ and $\mathrm{OD}_{600\mathrm{nm}} = 0.1$ (since these entered stationary phase at lower OD values).

To remove noise before differentiating, the OD and fluorescence data was then filtered using a moving average filter. Given a signal with n measurements $\mathbf{y} = [y_1, y_2, \ldots, y_{n+1}]$ sampled at a constant period Δt, we apply the moving average filter as follow:

$$d_j = \sum_{r=-2}^{2} \frac{y_{j+r}}{5}, \quad \forall j \in [3, 4, \ldots, n-1],$$

where $\mathbf{d} = [d_1, d_2, \ldots, d_{n+1}]$ is our filtered signal with boundary points identical to those of $\mathbf{y}$ ($d_1 = y_1$ and $d_2 = y_2$).

The growth rate μ is calculated from the filtered OD signal by performing linear regression (in a least-squares sense) on the log of the signal and taking the slope of the fit. The RFP and GFP production rates were calculated in a similar manner as [46]. Denoting $\mathrm{GFP}(t_i)$ and $\mathrm{RFP}(t_i)$ as the filtered GFP and RFP signal measured by the plate reader at time t_i, the GFP production rate ($\alpha_{\mathrm{GFP}}(t_i)$) and RFP production rate ($\alpha_{\mathrm{RFP}}(t_i)$) are given by

$$\alpha_{\mathrm{GFP}}(t_i) = \frac{\mathrm{GFP}(t_{i+1}) - \mathrm{GFP}(t_{i-1})}{2(t_{i+1} - t_{i-1})\mathrm{OD}(t_i)}, \quad \alpha_{\mathrm{RFP}}(t_i) = \frac{\mathrm{RFP}(t_{i+1}) - \mathrm{RFP}(t_{i-1})}{2(t_{i+1} - t_{i-1})\mathrm{OD}(t_i)},$$

where $\mathrm{OD}(t_i)$ is the filtered OD level.

References

[1] S. Cardinale and A. P. Arkin, "Contextualizing context for synthetic biology - identifying causes of failure of synthetic biological systems," *Biotechnol. J.*, vol. 7, no. 7, pp. 856–866, 2012.

[2] D. Del Vecchio, "Modularity, context-dependence, and insulation in engineered biological circuits," *Trends Biotechnol.*, vol. 33, no. 2, pp. 111–119, 2015.

[3] J. Vind, M. A. Sørensen, M. D. Rasmussen, and S. Pedersen, "Synthesis of proteins in Escherichia coli is limited by the concentration of free ribosomes. Expression from reporter genes does not always reflect functional mRNA levels.," 1993.

[4] A. Gyorgy, J. I. Jiménez, J. Yazbek, H. H. Huang, H. Chung, R. Weiss, and D. Del Vecchio, "Isocost Lines Describe the Cellular Economy of Genetic Circuits," *Biophys. J.*, vol. 109, no. 3, pp. 639–646, 2015.

[5] Y. Qian, H. H. Huang, J. I. Jiménez, and D. Del Vecchio, "Resource Competition Shapes the Response of Genetic Circuits," *ACS Synth. Biol.*, vol. 6, no. 7, pp. 1263–1272, 2017.

[6] I. Shachrai, A. Zaslaver, U. Alon, and E. Dekel, "Cost of Unneeded Proteins in E. coli Is Reduced after Several Generations in Exponential Growth," *Mol. Cell*, vol. 38, no. 5, pp. 758–767, 2010.

[7] M. S. Bienick, K. W. Young, J. R. Klesmith, E. E. Detwiler, K. J. Tomek, and T. A. Whitehead, "The interrelationship between promoter strength, gene expression, and growth rate," *PLoS One*, vol. 9, no. 10, 2014.

[8] F. Ceroni, R. Algar, G.-B. Stan, and T. Ellis, "Quantifying cellular capacity identifies gene expression designs with reduced burden," *Nat. Methods*, vol. 12, no. 5, pp. 415–418, 2015.

[9] C. W. Johnston and J. J. Collins, "Engineering microbial peer pressure," *Science (80-.).*, vol. 365, no. 6457, pp. 986–987, 2019.

[10] M. Manhart and E. I. Shakhnovich, "Growth tradeoffs produce complex microbial communities on a single limiting resource," *Nat. Commun.*, vol. 9, no. 1, 2018.

[11] N. S. McCarty and R. Ledesma-Amaro, "Synthetic Biology Tools to Engineer Microbial Communities for Biotechnology," 2019.

[12] L. Pacciani-Mori, S. Suweis, A. Maritan, and A. Giometto, "Constrained proteome allocation affects coexistence in models of competitive microbial communities," *ISME J.*, 2021.

[13] F. Ceroni, A. Boo, S. Furini, T. E. Gorochowski, O. Borkowski, Y. N. Ladak, A. R. Awan, C. Gilbert, G. B. Stan, and T. Ellis, "Burden-driven feedback control of gene expression," *Nat. Methods*, vol. 15, no. 5, pp. 387–393, 2018.

[14] A. P. Darlington, J. Kim, J. I. Jiménez, and D. G. Bates, "Dynamic allocation of orthogonal ribosomes facilitates uncoupling of co-expressed genes," *Nat. Commun.*, vol. 9, no. 1, 2018.

[15] H. H. Huang, Y. Qian, and D. Del Vecchio, "A quasi-integral controller for adaptation of genetic modules to variable ribosome demand," *Nat. Commun.*, vol. 9, no. 1, pp. 1–12, 2018.

[16] S. K. Aoki, G. Lillacci, A. Gupta, A. Baumschlager, D. Schweingruber, and M. Khammash, "A universal biomolecular integral feedback controller for robust perfect adaptation," *Nature*, vol. 570, no. 7762, pp. 533–537, 2019.

[17] J. Keener and M. Nomura, "Regulation of Ribosome Synthesis," *Escherichia coli Salmonella Cell. Mol. Biol.*, pp. 1417–1431, 1996.

[18] B. J. Paul, W. Ross, T. Gaal, and R. L. Gourse, "rRNA transcription in Escherichia coli," *Annu. Rev. Genet.*, vol. 38, pp. 749–770, 2004.

[19] K. Potrykus and M. Cashel, "Growth at best and worst of times," *Nat. Microbiol.*, vol. 3, no. 8, pp. 862–863, 2018.

[20] R. L. Gourse, T. Gaal, M. S. Bartlett, J. A. Appleman, and W. Ross, "rRNA TRANSCRIPTION AND GROWTH RATE–DEPENDENT REGULATION OF RIBOSOME SYNTHESIS IN ESCHERICHIA COLI," *Annu. Rev. Microbiol.*, vol. 50, no. 1, pp. 645–677, 1996.

[21] F. C. Neidhardt, "Bacterial growth: Constant obsession with dN/dt," *J. Bacteriol.*, vol. 181, no. 24, pp. 7405–7408, 1999.

[22] P. P. Dennis and H. Bremer, "Modulation of Chemical Composition and Other Parameters of the Cell at Different Exponential Growth Rates," *EcoSal Plus*, vol. 3, no. 1, 2008.

[23] M. Scott, E. M. Mateescu, Z. Zhang, and T. Hwa, "Interdependence of Cell Growth Origins and Consequences," *Science (80-.).*, vol. 330, no. November, pp. 1099–1102, 2010.

[24] E. Bosdriesz, D. Molenaar, B. Teusink, and F. J. Bruggeman, "How fast-growing bacteria robustly tune their ribosome concentration to approximate growth-rate maximization," *FEBS J.*, vol. 282, no. 10, pp. 2029–2044, 2015.

[25] P. P. Dennis, M. Ehrenberg, and H. Bremer, "Control of rRNA synthesis in Escherichia coli: a systems biology approach.," *Microbiol Mol Biol Rev*, vol. 68, no. 4, pp. 639–668, 2004.

[26] J. M. Zengel and L. Lindahl, "Diverse Mechanisms for Regulating Ribosomal Protein Synthesis in Escherichia coli," *Prog. Nucleic Acid Res. Mol. Biol.*, 1994.

[27] M. Schaechter, O. MaalOe, and N. O. Kjeldgaard, "Dependency on Medium and Temperature of Cell Size and Chemical Composition during Balanced Growth of Salmonella typhimurium," *J. Gen. Microbiol.*, 1958.

[28] J. A. Appleman, W. Ross, J. Salomon, and R. L. Gourse, "Activation of Escherichia coli rRNA transcription by FIS during a growth cycle," *J. Bacteriol.*, 1998.

[29] O. Schröder and R. Wagner, "The bacterial DNA-binding protein H-NS represses ribosomal RNA transcription by trapping RNA polymerase in the initiation complex," *J. Mol. Biol.*, 2000.

[30] T. Gaal, M. S. Bartlett, W. Ross, C. L. Turnbough, and R. L. Gourse, "Transcription regulation by initiating NTP concentration: rRNA synthesis in bacteria," *Science (80-.).*, 1997.

[31] D. A. Schneider, T. Gaal, and R. L. Gourse, "NTP-sensing by rRNA promoters in Escherichia coli is direct," *Proc. Natl. Acad. Sci. U. S. A.*, 2002.

[32] M. Cashel and J. Gallant, "Two compounds implicated in the function of the RC gene of escherichia coli," *Nature*, 1969.

[33] D. A. Schneider and R. L. Gourse, "Changes in the concentrations of guanosine 5-diphosphate 3-diphosphate and the initiating nucleoside triphosphate account for inhibition of rRNA transcription in fructose-1,6-diphosphate aldolase (fda) mutants," *J. Bacteriol.*, 2003.

[34] K. Potrykus, H. Murphy, N. Philippe, and M. Cashel, "ppGpp is the major source of growth rate control in E. coli," *Environ. Microbiol.*, vol. 13, no. 3, pp. 563–575, 2011.

[35] N. C. Imholz, M. J. Noga, N. J. van den Broek, and G. Bokinsky, "Calibrating the Bacterial Growth Rate Speedometer: A Re-evaluation of the Relationship Between Basal ppGpp, Growth, and RNA Synthesis in Escherichia coli," *Front. Microbiol.*, vol. 11, no. September, pp. 1–9, 2020.

[36] E. Sarubbi, K. E. Rudd, and M. Cashel, "Basal ppGpp level adjustment shown by new spoT mutants affect steady state growth rates and rrnA ribosomal promoter regulation in Escherichia coli," *MGG Mol. Gen. Genet.*, vol. 213, no. 2-3, pp. 214–222, 1988.

[37] M. Zacharias, H. U. Goringer, and R. Wagner, "Influence of the GCGC discriminator motif introduced into the ribosomal RNA P2- and tac promoter on growth-rate control and stringent sensitivity," *EMBO J.*, vol. 8, no. 11, pp. 3357–3363, 1989.

[38] P. P. Dennis and H. Bremer, "Modulation of Chemical Composition and Other Parameters of the Cell at Different Exponential Growth Rates," *EcoSal Plus*, vol. 3, no. 1, 2008.

[39] X. Dai and M. Zhu, "Coupling of Ribosome Synthesis and Translational Capacity with Cell Growth," *Trends Biochem. Sci.*, vol. 45, pp. 681–692, aug 2020.

[40] G. C. Atkinson, T. Tenson, and V. Hauryliuk, "The RelA/SpoT Homolog (RSH) superfamily: Distribution and functional evolution of ppgpp synthetases and hydrolases across the tree of life," *PLoS One*, vol. 6, no. 8, 2011.

[41] V. Hauryliuk, G. C. Atkinson, K. S. Murakami, T. Tenson, and K. Gerdes, "Recent functional insights into the role of (p)ppGpp in bacterial physiology," *Nat. Rev. Microbiol.*, vol. 13, no. 5, pp. 298–309, 2015.

[42] L. Fernández-Coll and M. Cashel, "Possible Roles for Basal Levels of (p)ppGpp: Growth Efficiency Vs. Surviving Stress," *Front. Microbiol.*, vol. 11, no. October, 2020.

[43] K. D. Murray and H. Bremer, "Control of spoT-dependent ppGpp Synthesis and Degradation in Escherichia coli," *J. Mol. Biol*, vol. 259, pp. 41–57, 1996.

[44] J. Ryals, R. Little, and H. Bremer, "Control of rRNA and tRNA syntheses in Escherichia coli by guanosine tetraphosphate," *J. Bacteriol.*, vol. 151, no. 3, pp. 1261–1268, 1982.

[45] D. R. Gentry and M. Cashel, "Mutational analysis of the Escherichia coli spoT gene identifies distinct but overlapping regions involved in ppGpp synthesis and degradation," *Mol. Microbiol.*, vol. 19, no. 6, pp. 1373–1384, 1996.

[46] F. Ceroni, R. Algar, G.-B. Stan, and T. Ellis, "Quantifying cellular capacity identifies gene expression designs with reduced burden," *Nat. Methods*, vol. 12, no. 5, pp. 415–418, 2015.

[47] V. J. Hernandez and H. Bremer, "Guanosine tetraphosphate (ppGpp) dependence of the growth rate control of rrnB P1 promoter activity in Escherichia coli," *J. Biol. Chem.*, vol. 265, no. 20, pp. 11605–11614, 1990.

[48] H. Xiao, M. Kalman, K. Ikehara, S. Zemel, G. Glaser, and M. Cashel, "Residual guanosine 3???,5???-bispyrophosphate synthetic activity of relA null mutants can be eliminated by spoT null mutations," *J. Biol. Chem.*, vol. 266, no. 9, pp. 5980–5990, 1991.

[49] K. Valgepea, K. Adamberg, A. Seiman, and R. Vilu, "Escherichia coli achieves faster growth by increasing catalytic and translation rates of proteins," *Mol. Biosyst.*, vol. 9, no. 9, p. 2344, 2013.

[50] M. Zhu, Y. Pan, and X. Dai, "(p)ppGpp: the magic governor of bacterial growth economy," *Curr. Genet.*, vol. 65, no. 5, pp. 1121–1125, 2019.

[51] V. J. Hernandez and H. Bremer, "Characterization of RNA and DNA synthesis in Escherichia coli strains devoid of ppGpp," *J. Biol. Chem.*, vol. 268, no. 15, pp. 10851–10862, 1993.

[52] M. Zhu, H. Mu, M. Jia, L. Deng, and X. Dai, "Control of ribosome synthesis in bacteria: the important role of rRNA chain elongation rate," *Sci. China Life Sci.*, vol. 3, pp. 169–84, aug 2020.

[53] F. Ceroni, S. Furini, T. E. Gorochowski, A. Boo, O. Borkowski, Y. N. Ladak, A. R. Awan, C. Gilbert, G.-B. Stan, and T. Ellis, "Burden-driven feedback control of gene expression," *bioRxiv*, pp. 1–17, 2017.

[54] D. Sun, G. Lee, J. H. Lee, H. Y. Kim, H. W. Rhee, S. Y. Park, K. J. Kim, Y. Kim, B. Y. Kim, J. I. Hong, C. Park, H. E. Choy, J. H. Kim, Y. H. Jeon, and J. Chung, "A metazoan ortholog of SpoT hydrolyzes ppGpp and functions in starvation responses," *Nat. Struct. Mol. Biol.*, vol. 17, no. 10, pp. 1188–1194, 2010.

[55] M. Zhu and X. Dai, "Growth suppression by altered (p)ppGpp levels results from non-optimal resource allocation in Escherichia coli," *Nucleic Acids Res.*, vol. 47, no. 9, pp. 4684–4693, 2019.

[56] R. Harinarayanan, H. Murphy, and M. Cashel, "Synthetic growth phenotypes of Escherichia coli lacking ppGpp and transketolase A (tktA) are due to ppGpp-mediated transcriptional regulation of tktB," *Mol. Microbiol.*, vol. 69, pp. 882–894, aug 2008.

[57] D. Del Vecchio, R. M. Murray, and D. Vecchio, *Biomolecular Feedback Systems*. 2010.

[58] A. G. Marr, "Growth Rate of Escherichia coli," *Microbiol. Mol. Biol. Rev.*, vol. 55, no. 2, pp. 316–333, 1991.

Supplementary Information

Detailed Experimental data

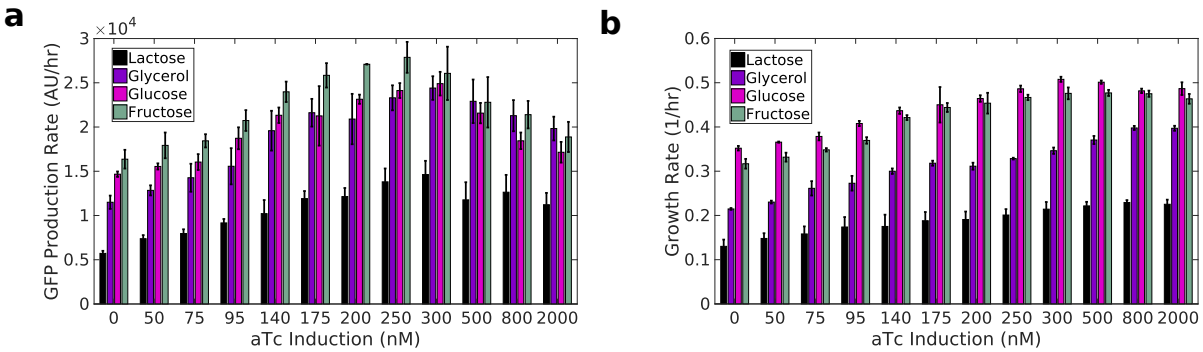

Figure 9: **The unnormalized data corresponding to the Fig. 2 in the main text (a)** Corresponding data to Fig. 2-d. **(b)** Corresponding data to Fig. 2-f.

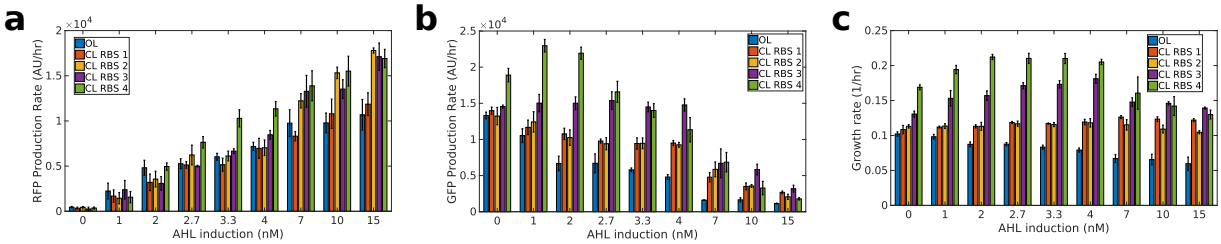

Figure 10: **The unnormalized data corresponding to the Fig. 4 in the main text for OL and CL in lactose (a)** Corresponding data to OL and CL in Fig. 4-f. **(b)** Corresponding data to OL and CL in Fig. 4-f. **(c)** Corresponding data to OL and CL in Fig. 4-g.

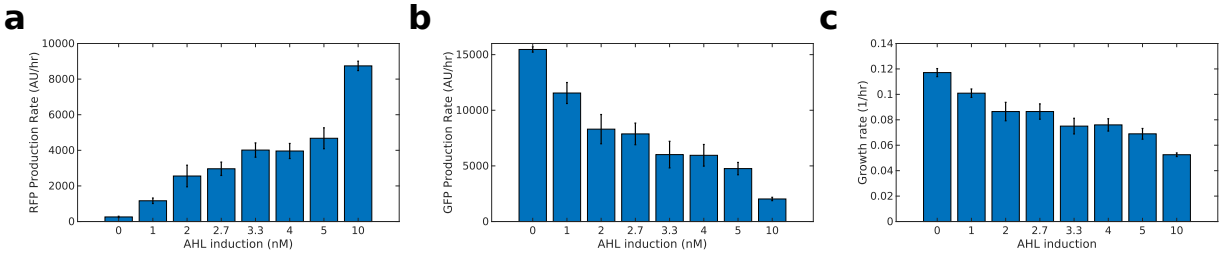

Figure 11: **The unnormalized data corresponding to the Fig. 4 in the main text for control in lactose (a)** Corresponding data to control in Fig. 4-f. **(b)** Corresponding data to control in Fig. 4-f. **(c)** Corresponding data to control in Fig. 4-g.

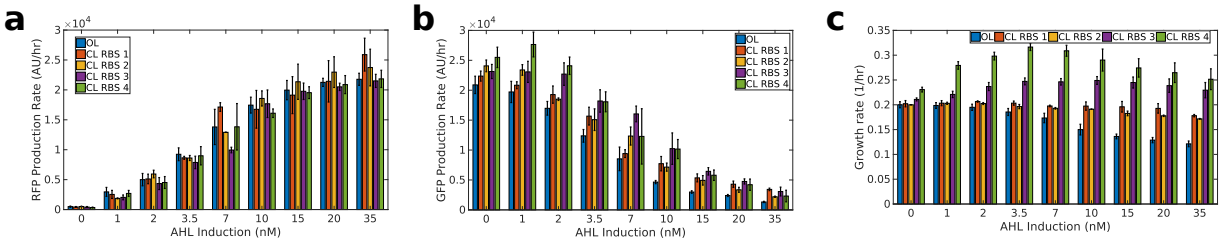

Figure 12: **The unnormalized data corresponding to the Fig. 4 in the main text for OL and CL in glycerol (a)** Corresponding data to OL and CL in Fig. 4-h. **(b)** Corresponding data to OL and CL in Fig. 4-h. **(c)** Corresponding data to OL and CL in Fig. 4-i.

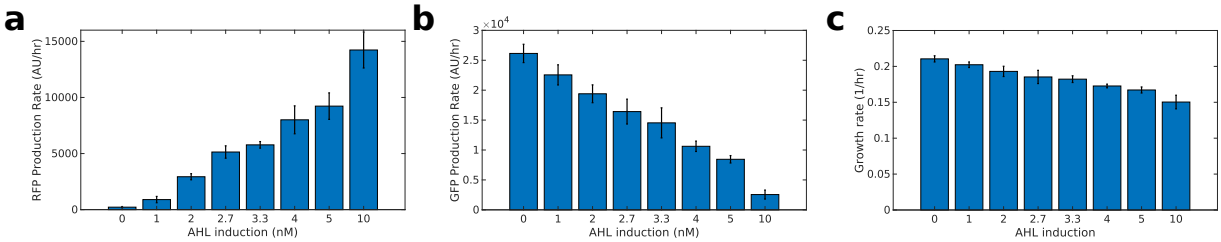

Figure 13: **The unnormalized data corresponding to the Fig. 4 in the main text for control in glycerol (a)** Corresponding data to control in Fig. 4-h. **(b)** Corresponding data to control in Fig. 4-h. **(c)** Corresponding data to control in Fig. 4-i.

SpoTH Actuator Model

Here we derive a model of the SpoTH actuator. We model spoTH mRNA being translated by ribosomes to produce the SpoTH protein, which catalyzes the hydrolysis of ppGpp. We model how ppGpp inhibits ribosome production and how this modifies the total ribosomal budget. This dimensional model contains many free parameters, but by nondimensionalizing the equations, we can reduce our governing equation to contain only two dimensionless parameters. Finally, we modify the equations to account for the expression of a heterologous protein.

SpoTH expression

We model spoTH mRNA ($\mathrm{m_s}$) binding to free ribosomes (R) to produce the translation initiation complex $\mathrm{c_s}$, which is then translated to produce the SpoTH protein S with elongation rate constant κ_s. The mRNA decays with rate constants δ_s and the protein dilutes with rate constant γ_s. The corresponding chemical reactions are:

$$\emptyset \xrightarrow{\alpha_s} \mathrm{m_s}, \quad \mathrm{m_s} \xrightarrow{\delta_s} \emptyset, \quad \mathrm{m_s} + \mathrm{R} \underset{\mathrm{d_s}}{\overset{\mathrm{a_s}}{\rightleftharpoons}} \mathrm{c_s} \xrightarrow{\kappa_s} \mathrm{m_s} + \mathrm{R} + \mathrm{P_s}, \quad \mathrm{S} \xrightarrow{\gamma_s} \emptyset, \tag{6}$$

where α_s is the production rate constant of the mRNA, a_s and d_s are the association and dissociation rate constant, respectively, between ribosomes and mRNA. Levering reaction rate equations, consequently, the concentration of each species satisfies:

$$\begin{aligned} \frac{dm_s}{dt} &= \alpha_s - a_s R m_s + (d_s + \kappa_s) c_s - \delta_s m_s, \\ \frac{dc_s}{dt} &= a_s R m_s - (d_s + \kappa_s) c_s \\ \frac{dS}{dt} &= \kappa_s c_s - \gamma_s P_s. \end{aligned} \tag{7}$$

The steady state of (7) is given by

$$m_s = \frac{\alpha_s}{\delta_s}, \quad c_s = \frac{m_s}{K_s} R, \quad S = \frac{\kappa_s}{\gamma_s} c_s, \tag{8}$$

where $K_s = \frac{d_s + \kappa_s}{a_s}$. From (8), the concentration of spoTH S is proportional to c_s (the number of ribosomes translating spoTH mRNA). The models (7) and (8) are consistent with [5].

ppGpp hydrolyzed by SpoTH

We now relate ppGpp concentration to SpoTH expression. We model ppGpp (G) being produce at a rate α_G, decayed at basal rate γ_{G_0}, and catalyzed by spoTH to GTP/GDP (G_p) at a rate a_G. The production rate α_G should

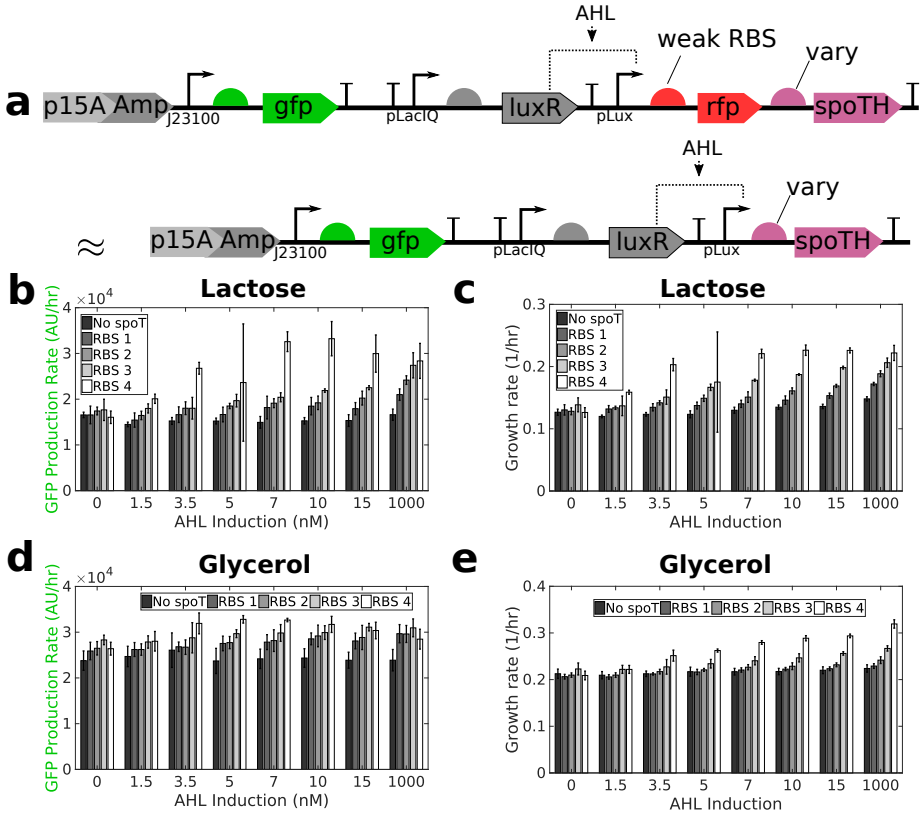

Figure 14: **SpoTH RBS library (a)** The genetic construct used to test the SpoTH RBS library. This construct is identical to Fig. 4-a in the main text, but with a very weak RFP RBS. For the entry labeled "No spoT" in the legends, the construct is identical but without the SpoTH RBS and CDS. **(b)** For lactose, the GFP production rate as SpoTH is expressed (increase AHL) for the RBS library. **(c)** For lactose, the growth rate as SpoTH is expressed (increase AHL) for the RBS library. **(d)** For glycerol, the GFP production rate as SpoTH is expressed (increase AHL) for the RBS library. **(e)** For glycerol, the growth rate as SpoTH is expressed (increase AHL) for the RBS library. For all data, error bars represent standard deviation from at least four replicates (two biological replicates each with two technical replicates).

be determined by the synthesis rate of relA and spoT. Similarly the basal decay rate γ_{G_0}, should have a contribution from the hydrolysis domain of spoT. The corresponding biochemical reactions are:

$$\emptyset \xrightarrow{\alpha_G} \mathrm{G}, \quad \mathrm{G} \xrightarrow{\gamma_{G_0}} \emptyset, \quad \mathrm{S} + \mathrm{G} \xrightarrow{a_G} \mathrm{G_P} + \mathrm{S}. \tag{9}$$

Notice that for simplicity we used a one step catalytic reaction [57] for the hydrolysis of ppGpp . The concentration of each species satisfies:

$$\frac{dG}{dt} = \alpha_G - \gamma_G G S - \gamma_{G_0} G. \tag{10}$$

The steady state of (10) is given by

$$G = \frac{G_0}{1 + S/K_{gs}}, \tag{11}$$

where $G_0 = \alpha_G/\gamma_{G_0}$ and $K_{gs} = \gamma_{G_0}/a_G$.

ppGpp represses ribosome production and SpoTH sequesters ribosomes

Next we show how ppGpp represser ribosome production and how the expression of SpoTH sequesters ribosomes. Denoting R_T as the concentrtion of the total ribosomes in the cell, we have that

$$R_T = R + c_s + c_e, \tag{12}$$

where c_e is the concentration of ribosome translating endogenous mRNA. From (12), it is clear that expressing spoTH (increasing c_s) should lower the number of free ribosomes. The total ribosome concentration obeys

$$\frac{dR_T}{dt} = \alpha_r - \gamma_r R_T, \tag{13}$$

where α_r is the ribosome production rate and γ_r is the ribosome decay rate. ppGpp represses ribosome production (via inhibition of rRNA), we model this repression by

$$\alpha_r = \frac{\alpha_r^*}{1 + (G/K_G)^2},$$

where K_G and α_r^* is the ribosome production rate in the absence of ppGpp. We use a hill coefficient of 2, consistent with [6, 58]. Taking the steady state of (13), we have that

$$R_T = \frac{R_T^*}{1 + (G/K_G)^2},$$

where $R_T^* = \alpha_r/\gamma_r$.

Dimensionless actuator model

We assume that c_e has a similar form as c_s in (8) such that

$$c_e = \frac{m_e}{K_e} R,$$

where m_e is the total endogenous mRNA and K_e is the effective dissociation constant of endogenous mRNA with ribosomes. We can rewrite (12) as

$$\frac{R_T^*}{1 + (G/K_G)^2}, = R(1 + \frac{m_e}{K_e}) + c_s, \implies \frac{1}{1 + (G/K_G)^2}, = \frac{R}{R_T^*}(1 + \frac{m_e}{K_e}) + \frac{c_s}{R_T^*},$$

and can be further expressed as:

$$\frac{1}{1 + (G_0/K_G)^2} + \Big[\frac{1}{1 + (G/K_G)^2} - \frac{1}{1 + (G_0/K_G)^2}\Big] = \frac{R}{R_T^*}(1 + \frac{m_e}{K_e}) + \frac{c_s}{R_T^*}. \tag{14}$$

Defining $\bar{R} = \frac{R}{R_T^*}(1 + \frac{m_e}{K_e})$ and $\bar{c}_s = c_s/R_T^*$ and using the relationship (11) and (8), we can express (14) in dimensionless form as

$$R_0 + (1 - R_0) f(\bar{c}_s/\epsilon, R_0) = \bar{R} + \bar{c}_s, \tag{15}$$

where

$$\theta_G = G_0/K_G, \quad R_0(\theta_G) = \frac{1}{1 + \theta_G^2}, \quad \epsilon = \frac{K_{gs}}{R_T^*}\frac{\gamma_s}{\kappa_s}, \quad f(\bar{c}_s/\epsilon, R_0) = \frac{(\bar{c}_s/\epsilon + 1)^2 - 1}{(\bar{c}_s/\epsilon + 1)^2 - 1 + 1/R_0}. \tag{16}$$

The dimensionless parameter θ_G is a measure of the basal ppGpp in the cell, R_0 is the free ribosome concentration (normalized by R_T^*) when no spoTH is expressed ($c_s = 0$) ϵ is the ribosomal cost to express sufficient spoTH to

degrade ppGpp (cost to actuate). A small ϵ implies that the amount of ribosomes needed to produce enough SpoTH to actuate (degrade a sufficient amount of ppGpp) is small compared to the increase in ribosomes due to ppGpp hydrolysis. Also notice that there is a monotonically decreasing relationship between the basal ppGpp θ_G and the nominal ribosome level R_0. Finally, a key parameter to determine the qualitative behavior of (15) is given by:

$$\delta(R_0, \epsilon) := \left.\frac{dR}{dc_s}\right|_{c_s=0} = 2\frac{\theta_G^2}{(1+\theta_G^2)^2\epsilon} - 1 = \frac{2R_0(1-R_0)}{\epsilon} - 1, \tag{17}$$

where $\delta \in (-1, \infty)$. By definition, if $\delta > 0$, it implies that ribosome levels increase as a small amount of exogenous SpoT is expressed.

Appending model with the expression of an additional heterologous protein

We model the mRNA of a heterologous protein ($\mathrm{m_y}$) binding to free ribosomes (R) to produce the translation initiation complex $\mathrm{c_y}$, which is then translated to produce the protein y with elongation rate constant κ_y. The mRNA decays with rate constants δ_y and the protein dilutes with rate constant γ_y. The corresponding chemical reactions are:

$$\emptyset \xrightarrow{\alpha_y} \mathrm{m_y}, \quad \mathrm{m_y} \xrightarrow{\delta_y} \emptyset, \quad \mathrm{m_y + R} \underset{\mathrm{d_y}}{\overset{\mathrm{a_y}}{\rightleftharpoons}} \mathrm{c_y} \xrightarrow{\kappa_y} \mathrm{m_y + R + P_y}, \quad \mathrm{y} \xrightarrow{\gamma_y} \emptyset, \tag{18}$$

where α_y is the production rate constant of the mRNA, a_y and d_y are the association and dissociation rate constant, respectively, between ribosomes and mRNA. The concentration of each species satisfies:

$$\begin{aligned} \frac{dm_y}{dt} &= \alpha_y - a_y R m_y + (d_y + \kappa_y)c_y - \delta_y m_y, \\ \frac{dc_y}{dt} &= a_y R m_y - (d_y + \kappa_y)c_y \\ \frac{dy}{dt} &= \kappa_y c_y - \gamma_y P_y. \end{aligned} \tag{19}$$

The steady state of (19) is given by

$$m_y = \frac{\alpha_y}{\delta_y}, \quad c_y = \frac{m_y}{K_y}R, \quad y = \frac{\kappa_y}{\gamma_y}c_y, \tag{20}$$

where $K_y = \frac{d_y+\kappa_y}{a_y}$.

We modify (12) to read

$$R_T = R + c_s + c_e + c_y.$$

Defining $\bar{c}_y = c_y/R_T^*$, we can write the total ribosme concentation in dimensionless from as in (15) as

$$R_0 + (1-R_0)f(\bar{c}_s/\epsilon, R_0) = \bar{R} + \bar{c}_s + \bar{c}_y, \tag{21}$$

When y and spoTH are under the same promoter, it implies $m_y = m_s$ and thus

$$c_s = \gamma c_y, \quad \gamma = K_s/K_y.$$

For this we have:

$$\left.\frac{dR}{dc_y}\right|_{c_y=0} = \frac{\gamma}{\delta} - 1. \tag{22}$$

Thus the inital can be made flat if:

$$\gamma = \delta(R_0, \epsilon). \tag{23}$$

The qualitative behavior of (21) when $c_s = \gamma c_y$ is shown in Fig. 15

Plasmid maps and DNA sequences

Part	Sequence (5' to 3') or biobricks part number
RBS 1	GTTACAGCTTAGCCCGATCCATTT
RBS 2	TGAGCGCCGCCAGGGACCACGC
RBS 3	CTCGACACACCCCCTATTAAAT
RBS 4	CAAACCTCTACCGTAGGATTCGTCATT

SpoTH	ATGTATCTGTTTGAAAGCCTGAATCAACTGATTCAAACCTACCTGCCGGAAGACCAAATCAAGCGTCTG CGGCAGGCGTATCTCGTTGCACGTGATGCTCACGAGGGGCAAACACGTTCAAGCGGTGAACCCTATATC ACGCACCCGGTAGCGGTTGCCTGCATTCTGGCCGAGATGAAACTCGACTATGAAACGCTGATGGCGGCG CTGCTGCATGACGTGATTGAAGATACTCCCGCCACCTACCAGGATATGGAACAGCTTTTTGGTAAAAGC GTCGCCGAGCTGGTAGAGGGGGTGTCGAAACTTGATAAACTCAAGTTCCGCGATAAGAAAGAGGCGCA GGCCGAAAACTTTCGCAAGATGATTATGGCGATGGTGCAGGATATCCGCGTCATCCTCATCAAACTTGC CGACCGTACCCACAACATGCGCACGCTGGGCTCACTTCGCCCGGACAAACGTCGCCGCATCGCCCGTGA AACTCTCGAAATTTATAGCCCGCTGGCGCACCGTTTAGGTATCCACCACATTAAAACCGAACTCGAAGA GCTGGGTTTTGAGGCGCTGTATCCCAACCGTTATCGCGTAATCAAAGAAGTGGTGAAAGCCGCGCGCCA AAATTCGTCAGTTGCTGAAAAACCTCAAGCGTAATAA
CJB	ATGcatcatcatcatcatcatGCGTCGAAAATCTCAGACAATGTACGTATTAAACTGTACATGGAAGGCACCGTCA ACAACCATCACTTCATGTGTGAAGCGGAAGGTGAAGGCAAGCCGTACGAAGGAACCCAGATGGAAAACA TTAAAGTCACTAAAGGTGGCCCTCTTCCGTTCTCTTTCGACATTCTCACGCCGAACTGTCAGTATGGGT CAGTGGCAATCACCAAATATACCAGTGGCATCCCGGACTACTTTAAGCAGAGCTTTCCTGAGGGATTCA CGTGGGAACGCACGACCATCTATGAAGACGGGGCCTACCTTACAACCCAACAAGAAACGAAGCTTGACG GCAACTGCCTGGTGTATAACATCAAGATTCTGGGTTGCAATTTCCCACCGAACGGCCCGGTGATGCAGA AGAAAACACAGGGATGGGAACCCTGTTGCGAGATGCGTTATACACGTGATGGAGTATTGTGTGGGCAG ACACTTATGGCGCTCAAATGTGCAGATGGGAACCACCTCACTTGCCACTTACGCACGACGTACCGCTCC AAAAAAGCGGCAAAGGCGCTGCAGATGCCGCCGTTCCATTTCAGTGACTCACGCCCTGAGATCGTGAAA GTTAGCGAGAATGGAACTCTTTTCGAACAGCATGAATCCTCAGTGGCCCGCTATTGCCAAACGTGTCCT TCCAAACTCGGCCATAACTAATAA

Table 1: Essential DNA sequences used in this study

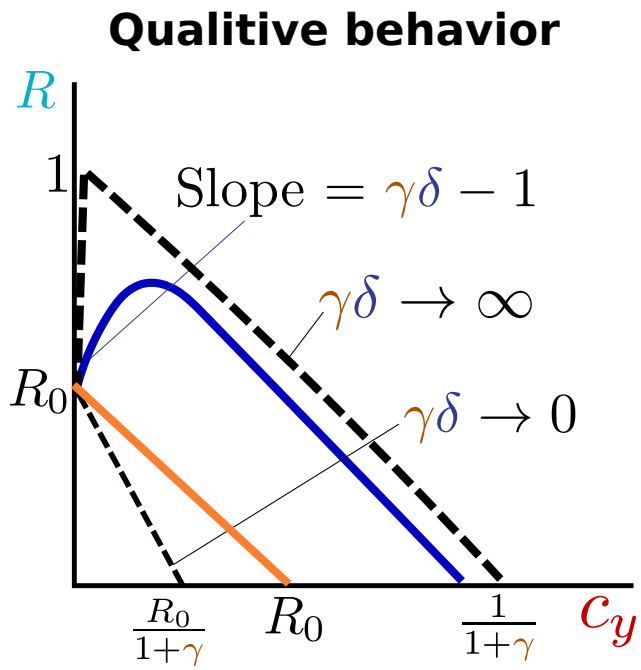

Figure 15: **The qualitative behavior coexpressing** y **and SpoTH under the same promoter** The qualitative behavior of (21) when $c_s = \gamma c_y$ (blue line). The open loop ($c_s = 0$ for all c_y) is shown in orange. The asymptotic behavior as $\gamma\delta \to 0$ and $\gamma\delta \to \infty$ are shown in dashed lines.

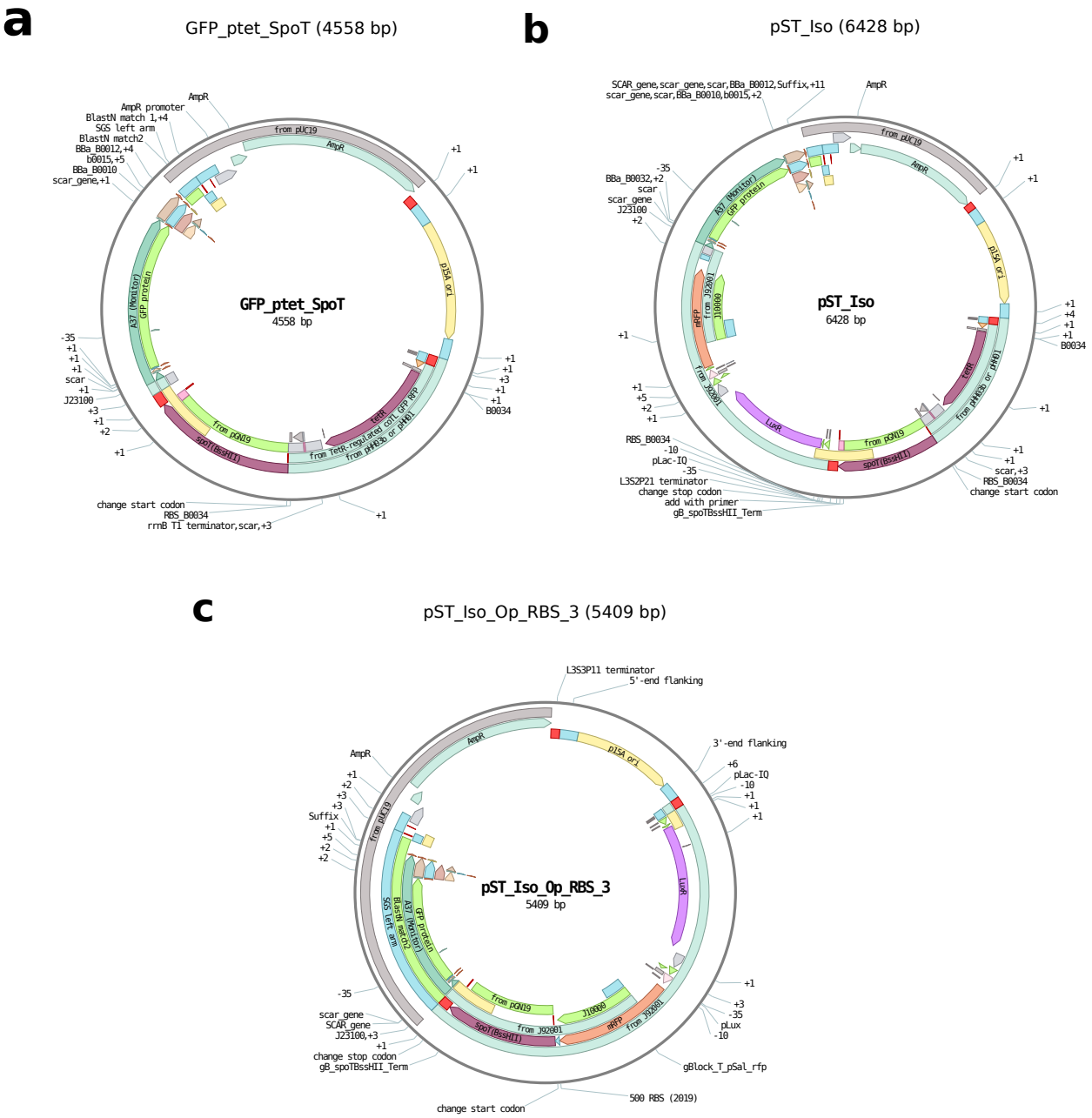

Figure 16: **Plasmid maps (a)** The genetic construct map for the construct for Fig. 2-a in the main text. **(b)** The genetic construct map for the construct for Fig. 3-a in the main text. **(c)** The genetic construct map for the construct for Fig. 4-c (No spoT), Fig. 4-d, Fig. 4-c (replace spoT with CJB) in the main text.